TWO- AND THREE-DIMENSIONAL INSTABILITIES

OF CONFINED FLOWS:

NUMERICAL STUDY BY A GLOBAL GALERKIN METHOD

Alexander Yu. GELFGAT

Computational Mechanics Laboratory, Faculty of Mechanical Engineering,
Technion - Israel Institute of Technology, Haifa 32000, Israel
e-mail: alexg@cmlp.technion.ac.il

Abstract

A version of the global Galerkin method applied to a wide range of hydrodynamic stability problems is described. The numerical algorithm is based on a non-orthogonal set of globally defined basis functions, which satisfy all linear boundary conditions and the continuity equation. This leads to a significant reduction of the number of scalar degrees of freedom of the numerical model. The relatively low number of degrees of freedom makes it possible to solve the eigenvalue problem associated with the linear stability of flow, and to approximate asymptotically the slightly supercritical flows that arise after the onset of instability. The main objective is the analysis of stability of steady state flows which are calculated numerically. Details and advantages of the proposed approach are illustrated on several examples.

1. INTRODUCTION

Consider a steady state flow obtained as a numerical solution of a time-dependent fluid dynamics problem, which includes equations of momentum and continuity, together with transport of heat and mass, chemical reactions, electrodynamics, etc. The flow is defined by several governing parameters (Reynolds number, Prandtl number, Schmidt number, etc.). Obviously, for some parameter values this solution can be unstable or non-unique. There are two main ways to study the stability of a numerically calculated steady state flow. The first and most common is the straight-forward integration in time with a small perturbation added to the steady solution. The second and more rigorous is the investigation of the stability properties by studying the spectrum of the corresponding linearized problem. The first approach is usually so CPU-time consuming that it becomes impossible to study the stability in a wide parameter range. Furthermore, the characteristic time of the dominant perturbation of the problem (amplification increment, frequency of oscillations) is not known *a priori*, which causes additional problems related to the correct choice of the time step. The second approach leads to an eigenvalue problem whose size is equal to the number of degrees of freedom of the numerical method. Usually, this size (equal to the number of discretization elements multiplied by the number of unknown functions) is very large. For example, a two-dimensional CFD problem, being solved on a 100×100 grid, results in 30,000 degrees of freedom. Solution of such problems became possible only recently. It requires the implementation of Krylov subspace iteration methods [1] and still leads to heavily CPU-time consuming calculations.

An alternative approach was proposed in [2],[3] and is described here in some more detail. The idea is to apply a global spectral approach and in this way to avoid the discretization of the flow region. If the basis functions are chosen appropriately then the spectral convergence of the corresponding Galerkin series will be reached and finally a lesser number of degrees of freedom will be needed for the approximation of the solution. The global spectral methods, applied to the Navier-Stokes and transport equations usually require a too large computer memory and for this reason remained impractical for many years. Recently, however, the available computer memory became rather large (e.g., more than 1 Gbyte memory is available for a personal workstation) and is growing rapidly. Therefore, it becomes possible to apply the global spectral methods to complicated fluid dynamic problems.

Clearly, the efficiency of a spectral method is determined by the choice of the basis functions. It is very desirable to include the boundary conditions and possibly other properties of the

solution into a spectral series before the computational process starts (e.g., the incompressible continuity equation can be solved by the use of a divergent-free basis). This can be done in the case when the flow region is an arbitrary canonical domain, i.e., a domain whose borders are coordinate surfaces, for an arbitrary set of linear boundary conditions. A possible way to define such basis and several examples of scalar and vector sets of the basis functions are given in Section 2. Some details of the numerical implementation, which includes the calculation of steady flows, study of their stability and asymptotic approximation of supercritical flows are described in Section 3. Section 4 contains some examples of successful use of the described approach.

This paper was presented as a keynote lecture at the 8th International Symposium of Computational Fluid Dynamics. Different variations of the described numerical approach and main results are published in [2]-[10]. The main objective of the present paper is to give a complete and systematic description of the numerical approach, which can be used for a wide variety of problems.

2. BASIS FUNCTIONS

2.1 Basis Functions Satisfying Boundary Conditions.

Consider an arbitrary one-dimensional problem, defined in the interval $x \in [x_1, x_2]$. Assume also that N boundary conditions of the problem are linear and homogeneous. These boundary conditions can be represented as

$$\sum_{l=1}^{L} \alpha_{ml} u^{(l)}(x)\Big|_{x=x_1,x_2} = 0, \quad m = 1,2,3, \ldots, N \tag{1}$$

where $u(x)$ is the unknown function, α_{ml} are arbitrary coefficients, the superscript (l) denotes derivatives, and x has the value of x_1 or x_2 (a negative value of l can be interpreted as the integral from x_1 to x_2). Suppose also that the solution u belongs to a Banach space W, and a system of functions $\{\psi_n(x)\}_{n=0}^{\infty} \in W$ forms a basis in W. We assume that this basis can be efficiently used to approximate the unknown solution by a truncated series

$$u(x) \approx \sum_{m=0}^{M} a_m \psi_m(x) \tag{2}$$

In the general case the functions $\psi_k(x)$ do not satisfy the boundary conditions (1) and special care should be taken to satisfy them (e.g. weak formulation, tau-spectral approach). Usually this slows down the convergence. On the other hand, all functions satisfying (1) form a subspace $U \subseteq W$. Obviously, $u(x) \in U$ and one can expect that the use of a basis in U, instead of a basis in W, will provide a faster convergence. To construct the basis in U from the more general basis $\{\psi_n(x)\}_{n=0}^{\infty} \in W$, we consider linear superpositions of the functions $\psi_n(x)$

$$\varphi_n(x) \approx \sum_{i=0}^{N} b_{ni} \psi_{n+i}(x), \tag{3}$$

i.e., for N boundary conditions (1) we define the superpositions of $N+1$ basis functions $\psi_n(x)$. Each n-th superposition contains the functions $\psi_{n+i}(x)$ with the index varying from n to $n+N$. Substitution of (3) in (1) yields ($m = 1,2,3, \ldots, N$):

$$0 = \sum_{l=1}^{L} \alpha_{ml} \varphi_n^{(l)}(x) \Big|_{x=x_1,x_2} = \sum_{l=1}^{L} \alpha_{ml} \sum_{i=0}^{N} b_{ni} \psi_{n+i}^{(l)}(x) \Big|_{x=x_1,x_2} = \sum_{i=0}^{N} b_{ni} \sum_{l=1}^{L} \alpha_{ml} \psi_{n+i}^{(l)}(x) \Big|_{x=x_1,x_2} \tag{4}$$

Relation (4) defines N linear homogeneous algebraic equations for the $N+1$ coefficients b_{ni} ($i = 0,1,2, \ldots, N$) for each fixed index n:

$$\sum_{i=0}^{N} A_{mi} b_{ni} = 0, \qquad A_{mi} = \sum_{l=1}^{L} \alpha_{ml} \psi_{n+i}^{(l)}(x) \Big|_{x=x_1,x_2}, \qquad m = 1,2,3, \ldots, N \tag{5}$$

To make this system definite one can assign the value $b_{n0} = 1$ and obtain the other b_{ni} ($i = 1,2, \ldots, N$) from (5). This will provide a unique solution for all coefficients b_{ni} if the boundary conditions (1) are independent. The functions $j_n(x)$ defined in this way satisfy the boundary conditions (1). It is easy to prove that the system $\{\varphi_n\}_{n=0}^{\infty} \in U \subseteq W$ forms a basis in the subspace U. The coefficients b_{ni} should be obtained analytically, as functions of the indices n and i, before the computational process starts (examples for some particular boundary conditions are given below). This can be easily done with the help of computer algebra. The unknown solution $u(x)$ can be now approximated as

$$u(x) \approx \sum_{k=0}^{K} a_k \varphi_k(x) \tag{6}$$

The truncated series (6) satisfies the boundary conditions (1) analytically for any truncation number K. The functions $j_n(x)$ can be used as trial functions for a general weighted residuals method. In case of the classical Galerkin method the weight functions coincide with $j_n(x)$. In the most general case $y_n(x)$ should be used as the weight functions. However, if the residual satisfies some linear homogeneous boundary conditions, a similar procedure can be used to make the projection on the corresponding subspace and to choose the weight functions which satisfy the boundary conditions.

Note, that the described procedure does not preserve orthogonality of the initial basis functions $y_n(x)$, in the case when these were orthogonal. The functions $j_n(x)$ can be orthogonalized, if necessary, using the Gram-Schmidt orthogonalization procedure. However for non-linear problems, when the evaluation of non-linear terms requires the largest computational effort, the orthogonality of basis functions is not very helpful.

We assume that the series (6) will converge faster (at least not slower) in the subspace U than the series (2) converges in the larger functional space W. However, this statement cannot be proved for a general case. The convergence must be carefully checked for each particular problem, as it was done in [2],[3],[8].

The process of constructing the basis is defined here only for the homogeneous boundary conditions (1). Furthermore, only in case of homogeneity the series (6) will satisfy the same boundary conditions. Therefore, we suppose that all inhomogeneities were removed by an appropriate change of variables, and the numerical process starts only after the boundary conditions were made homogeneous. Examples of such changes of the variables can be found in [2],[3],[9].

In the case of a multi-dimensional problem, defined in any orthogonal coordinates, the same procedure can be applied along each coordinate direction (see examples below). The only restriction is the shape of the domain, which has to be canonical, i.e., the boundaries of the domain must coincide with the coordinate surfaces. This restriction is rather strong and probably cannot be removed without some extension of the described approach beyond the classical Galerkin formulation (e.g., subdomain collocation, domain decomposition techniques, spectral element approach).

2.2 Examples of Basis Functions Based on Chebyshev Polynomials

To construct basis functions for different boundary value problems we shall use the shifted Chebyshev polynomials of the first and second kind defined in the interval $x \in [0,1]$

$$T_n(x) = cos[n\, arccos(2x-1)], \qquad U_n(x) = \frac{sin[(n+1)arccos(2x-1)]}{sin[arccos(2x-1)]} \qquad (7)$$

The two systems $\{T_n\}$ and $\{U_n\}$ form bases in $L_2[0,1]$. To define bases for different boundary conditions we need values of the polynomials and their derivatives at the ends of the interval:

$$T_n(0) = (-1)^n, \qquad\qquad\qquad T_n(1) = 1, \qquad\qquad (8)$$

$$U_n(0) = (-1)^n(n+1), \qquad\qquad U_n(1) = n+1 \qquad\qquad (9)$$

$$T_n'(0) = (-1)^n 2n^2, \qquad\qquad\qquad T_n'(1) = 2n^2, \qquad\qquad (10)$$

$$U_n'(0) = (-1)^n n(n+1)(n+2)/3, \qquad U_n'(1) = n(n+1)(n+2)/3 \qquad (11)$$

and a relation connecting both systems of polynomials:

$$T_n'(x) = 2(n+1)U_{n-1}(x) \qquad\qquad (12)$$

2.2.1 Two-point boundary value problem

Consider a two-point boundary value problem with the boundary conditions defined as

$$\alpha_0 u'(0) + \beta_0 u(0) = 0, \qquad\qquad \alpha_1 u'(1) + \beta_1 u(1) = 0 \qquad\qquad (13)$$

where α_0, β_0, α_1, and β_1 are known coefficients. We approximate the unknown function $u(x)$ as a series

$$u(x) \approx \sum_{i=0}^{N} a_i \varphi_i(x), \qquad \varphi_i(x) = T_i(x) + f_i^1 T_{i+1}(x) + f_i^2 T_{i+2}(x) \qquad (14)$$

To define the coefficients f_i^1 and f_i^2, we substitute (14) into the boundary conditions (13). This yields two linear algebraic equations for f_i^1 and f_i^2:

$$f_1^i\left[-\alpha_0(i+1)^2 - \beta_0\right] + f_2^i\left[\alpha_0(i+2)^2 + \beta_0\right] = -\alpha_0 i^2 - \beta_0$$

$$f_1^i\left[\alpha_1(i+1)^2 + \beta_1\right] + f_2^i\left[\alpha_1(i+2)^2 + \beta_1\right] = -\alpha_1 i^2 - \beta_1 \qquad\qquad (15)$$

These equations can be solved analytically, yielding:

$$f_1^i = -\frac{\left(\alpha_1 i^2 + \beta_1\right)\left[\alpha_0(i+2)^2 + \beta_0\right] - \left(\alpha_0 i^2 + \beta_0\right)\left[\alpha_1(i+2)^2 + \beta_1\right]}{\left[\alpha_0(i+1)^2 + \beta_0\right]\left[\alpha_1(i+2)^2 + \beta_1\right] + \left[\alpha_1(i+1)^2 + \beta_1\right]\left[\alpha_0(i+2)^2 + \beta_0\right]} \quad (16)$$

$$f_2^i = -\frac{\left(\alpha_0 i^2 + \beta_0\right)\left[\alpha_1(i+1)^2 + \beta_1\right] + \left(\alpha_1 i^2 + \beta_1\right)\left[\alpha_0(i+1)^2 + \beta_0\right]}{\left[\alpha_0(i+1)^2 + \beta_0\right]\left[\alpha_1(i+2)^2 + \beta_1\right] + \left[\alpha_1(i+1)^2 + \beta_1\right]\left[\alpha_0(i+2)^2 + \beta_0\right]} \quad (17)$$

Similar linear combinations of the Chebyshev polynomials were used in [11] for the solution of the one-dimensional Orr-Sommerfeld equation.

2.2.2 Basis functions for Poisson equation in cube

Consider the Poisson equation

$$\frac{\partial^2 u}{\partial x^2} + \frac{\partial^2 u}{\partial y^2} + \frac{\partial^2 u}{\partial z^2} = q(x, y, z) \quad (18)$$

in the cube $0 \leq x,y,z \leq 1$. To describe different possibilities let us define boundary conditions of the first, second and third type in the x-, y- and z- directions respectively:

$$u|_{x=0} = u|_{x=1} = 0, \qquad \left.\frac{\partial u}{\partial y}\right|_{y=0} = \left.\frac{\partial u}{\partial y}\right|_{y=1} = 0, \quad (19,20)$$

$$\left(u + \gamma\frac{\partial u}{\partial z}\right)_{z=0} = 0, \quad \left(u + \lambda\frac{\partial u}{\partial z}\right)_{z=1} = 0 \quad (21,22)$$

To construct the basis for $u(x,y,z)$ one should consider two-point boundary value problems in each direction separately and use eqs.(14,16,17) to construct basis functions in each direction. Then the one-dimensional basis functions should be combined into the three-dimensional ones. This yields:

$$u(x, y, z) \approx \sum_{i=0}^{N} \sum_{j=0}^{M} \sum_{k=0}^{K} a_{ijk}\varphi_i(x)\phi_j(y)\psi_k(z) \quad (23)$$

where

$$\varphi_i(x) = T_i(x) - T_{i+2}(x) \quad (26)$$

$$\phi_j(y) = T_j(y) - \frac{j^2}{(j+2)^2}T_{j+2}(y) \quad (27)$$

$$\psi_l(z) = T_l(z) - \frac{\left(i^2 + \lambda\right)\left[(i+2)^2 + \gamma\right] - \left(i^2 + \gamma\right)\left[(i+2)^2 + \lambda\right]}{\left[(i+1)^2 + \gamma\right]\left[(i+2)^2 + \lambda\right] + \left[(i+1)^2 + \lambda\right]\left[(i+2)^2 + \gamma\right]} T_{l+1}(z) -$$

$$- \frac{\left(i^2 + \gamma\right)\left[(i+1)^2 + \lambda\right] + \left(i^2 + \lambda\right)\left[(i+1)^2 + \gamma\right]}{\left[(i+1)^2 + \gamma\right]\left[(i+2)^2 + \lambda\right] + \left[(i+1)^2 + \lambda\right]\left[(i+2)^2 + \gamma\right]} T_{l+2}(z)$$

(28)

The solution of the problem (18)-(22) can be carried out by the classical Galerkin method if the functions (26)-(28) will be used as both trial and weight systems. Otherwise, for a general weighted residuals method, the weight system can be defined in a similar way.

2.2.3 Basis functions for a two-dimensional divergence-free vector field in Cartesian coordinates

The usual unknown functions in incompressible fluid dynamics are divergence-free vector fields. For an efficient application of a spectral method, we need a system of divergent-free basis functions that satisfy the boundary conditions. To derive such a system we first define a basis in a general space of divergence-free vector fields, and then apply the described procedure to satisfy the boundary conditions.

Recalling that both systems of Chebyshev polynomials $\{T_n\}$ and $\{U_n\}$ form bases in the space of scalar functions, and using the property (12), we define:

$$\mathbf{w}_{ij} = \begin{Bmatrix} w^{(x)} \\ w^{(y)} \end{Bmatrix} = \begin{Bmatrix} \dfrac{1}{2i} T_i(x)\, U_{j-1}(y) \\ -\dfrac{1}{2j} U_{i-1}(x)\, T_j(y) \end{Bmatrix}, \qquad i, j = 1,2,3, \dots , \qquad (29)$$

$$\mathbf{w}_{0j} = \begin{Bmatrix} \dfrac{1}{2} U_{j-1}(y) \\ 0 \end{Bmatrix}, \quad j = 1,2,3,\dots; \qquad \mathbf{w}_{i0} = \begin{Bmatrix} 0 \\ -\dfrac{1}{2} U_{i-1}(x) \end{Bmatrix}, \quad i = 1,2,3,\dots \qquad (30)$$

It can be shown that, according to (12), the two-dimensional divergence of all functions $\mathbf{w}_{ij}$ vanishes:

$$\nabla \cdot \mathbf{w}_{ij} = \frac{\partial w^{(x)}}{\partial x} + \frac{\partial w^{(y)}}{\partial y} = \frac{1}{2i} U_{j-1}(y)\frac{dT_i(x)}{dx} - \frac{1}{2j} U_{i-1}(x)\frac{dT_j(y)}{dy} =$$

(31)

$$= U_{j-1}(y)\, U_{i-1}(x) - U_{i-1}(x)\, U_{j-1}(y) = 0$$

Since both systems $\{T_n\}$ and $\{U_n\}$ form scalar bases, each component of $\mathbf{w}_{ij}$ is represented as a linear superposition of the scalar basis functions. Therefore, the vector functions (29),(30) form a basis in the space of divergent-free vector fields.

In the case of a problem in a two-dimensional rectangle $0 \le x \le A$, $0 \le y \le 1$ we have to satisfy 8 boundary conditions, i.e., one boundary condition for each component of the velocity field on each boundary, or 4 boundary conditions in each direction. According to the described procedure, we define a product of two linear superpositions of functions in the x- and y- directions, consisting of 5 (i.e., 4+1) scalar basis functions each:

$$
\mathbf{u}_{ij}(x, y) = \left\{
\begin{array}{c}
\dfrac{A}{2} \displaystyle\sum_{m=0}^{4} \dfrac{a_{im}}{(i+m)} T_{i+m}\left(\dfrac{x}{A}\right) \displaystyle\sum_{l=0}^{4} b_{jl} U_{j+l-1}(y) \\[3mm]
-\displaystyle\sum_{m=0}^{4} a_{im} U_{i+m-1}\left(\dfrac{x}{A}\right) \displaystyle\sum_{l=0}^{4} \dfrac{b_{jl}}{2(j+l)} T_{j+l}(y)
\end{array}
\right\}
\tag{32}
$$

Similarly to (31) one can show that $\nabla \cdot \mathbf{u}_{ij} = 0$. The coefficients a_{im} and b_{jl} should be chosen to satisfy the boundary conditions. For example, the boundary conditions defined for the velocity field $\mathbf{v}$ in [6] are

$$
\mathbf{v}\big|_{x=0} = \mathbf{v}\big|_{x=A} = \mathbf{v}\big|_{y=0} = \mathbf{0}, \qquad \frac{\partial v^{(x)}}{\partial y}\bigg|_{y=1} = v^{(y)}\big|_{y=1} = 0
\tag{33}
$$

Substitution of (32) into (33) and the analytical solution of the corresponding system of linear algebraic equations lead to the following coefficients a_{im} and b_{jl}:

$$
a_{i1} = a_{i3} = 0, \qquad a_{02} = -\frac{8}{3}, \qquad a_{04} = \frac{4}{3}
$$

$$
a_{i2} = -\frac{i}{i+2} - \frac{(i+1)(i+4)^2}{i(i+2)(i+3)}, \qquad a_{i4} = \frac{(i+1)(i+4)}{i(i+3)}, \qquad i > 0
\tag{34}
$$

$$b_{01} = \frac{2}{7}; \qquad b_{i1} = 2\frac{i^2 + 2i + 1}{i^3 + 5i^2 + 7i}, \qquad\qquad i > 0$$

$$b_{02} = -\frac{16}{7}; \qquad b_{i2} = -2\frac{i^4 + 8i^3 + 26i^2 + 40i + 24}{i^4 + 8i^3 + 22i^2 + 21i}, \qquad i > 0$$

$$b_{03} = -\frac{6}{7}; \qquad b_{i3} = -2\frac{i^2 + 4i + 3}{i^3 + 5i^2 + 7i}, \qquad\qquad i > 0 \tag{35}$$

$$b_{04} = \frac{4}{7}; \qquad b_{i4} = \frac{i^4 + 8i^3 + 22i^2 + 27i + 12}{i^4 + 8i^3 + 22i^2 + 21i}, \qquad i > 0$$

2.2.4 Basis functions for a three-dimensional divergence-free vector field in Cartesian coordinates

To approximate a three-dimensional divergent-free velocity field $\mathbf{v}$ it is necessary to define two independent systems of basis functions similar to (32). It follows from

$$\nabla \cdot \mathbf{v} = \frac{\partial v^{(x)}}{\partial x} + \frac{\partial v^{(y)}}{\partial y} + \frac{\partial v^{(z)}}{\partial z} = 0 \tag{36}$$

that $\mathbf{v}$ can be represented as

$$\mathbf{v} = \begin{pmatrix} v^{(x)} \\ v^{(y)} \\ v^{(z)} \end{pmatrix} = \begin{pmatrix} v^{(x)} \\ v^{(y)} \\ -\int\left(\frac{\partial v^{(x)}}{\partial x} + \frac{\partial v^{(y)}}{\partial y}\right)dz \end{pmatrix} = \begin{pmatrix} v^{(x)} \\ 0 \\ -\int\frac{\partial v^{(x)}}{\partial x}dz \end{pmatrix} + \begin{pmatrix} 0 \\ v^{(y)} \\ -\int\frac{\partial v^{(y)}}{\partial y}dz \end{pmatrix} \tag{37}$$

The two terms on the right hand side of (37) can be interpreted as the projections of the field $\mathbf{v}$ on the xy- $(y=const)$ and xz- $(x=const)$ planes respectively. Therefore, to represent the three-dimensional divergent-free vector field as a Galerkin series, it is necessary to define two independent sets of basis functions which will allow to approximate the projections of the velocity on these planes. The velocity $\mathbf{v}$ is approximated as

$$\mathbf{v} \approx \sum_{i=0}^{N_x} \sum_{j=0}^{N_y} \sum_{k=0}^{N_z} \left[c_{ijk}^{(x)} \mathbf{w}_{ijk}^{(x)}(x, y, z) + c_{ijk}^{(y)} \mathbf{w}_{ijk}^{(y)}(x, y, z) \right] \tag{38}$$

where $c_{ijk}^{(x)}$ and $c_{ijk}^{(y)}$ are unknown (possibly, time-dependent) coefficients, and $\mathbf{w}_{ijk}^{(x)}$ and $\mathbf{w}_{ijk}^{(y)}$ are the basis functions in the planes $x=const$ and $y=const$ respectively. For a three-dimensional rectangular region $0 \le x \le A_x$, $0 \le y \le A_y$, $0 \le z \le 1$ these functions can be defined as

$$
\mathbf{w}_{ijk}^{(x)}(x,y,z) = \left\{
\begin{array}{c}
0 \\[2mm]
\dfrac{A_y}{2} \displaystyle\sum_{\alpha=0}^{4} \tilde{f}_{i\alpha} T_{i+\alpha}(\dfrac{x}{A_x}) \sum_{\beta=0}^{4} \dfrac{\tilde{g}_{j\beta}}{(j+\beta)} T_{j+\beta}(\dfrac{y}{A_y}) \sum_{\gamma=0}^{4} \tilde{h}_{k\gamma} U_{k+\gamma-1}(z) \\[4mm]
-\dfrac{1}{2} \displaystyle\sum_{\alpha=0}^{4} \tilde{f}_{i\alpha} T_{i+\alpha}(\dfrac{x}{A_x}) \sum_{\beta=0}^{4} \tilde{g}_{j\beta} U_{j+\beta-1}(\dfrac{y}{A_y}) \sum_{\gamma=0}^{4} \dfrac{\tilde{h}_{k\gamma}}{(k+\gamma)} T_{k+\gamma}(z)
\end{array}
\right\} \tag{39}
$$

$$
\mathbf{w}_{ijk}^{(y)}(x,y,z) = \left\{
\begin{array}{c}
\dfrac{A_x}{2} \displaystyle\sum_{\alpha=0}^{4} \dfrac{\hat{f}_{i\alpha}}{(i+\alpha)} T_{i+\alpha}(\dfrac{x}{A_x}) \sum_{\beta=0}^{4} \hat{g}_{j\beta} T_{j+\beta}(\dfrac{y}{A_y}) \sum_{\gamma=0}^{4} \hat{h}_{k\gamma} U_{k+\gamma-1}(z) \\[4mm]
0 \\[2mm]
-\dfrac{1}{2} \displaystyle\sum_{\alpha=0}^{4} \hat{f}_{i\alpha} U_{i+\alpha-1}(\dfrac{x}{A_x}) \sum_{\beta=0}^{4} \hat{g}_{j\beta} T_{j+\beta}(\dfrac{y}{A_y}) \sum_{\gamma=0}^{4} \dfrac{\hat{h}_{k\gamma}}{(k+\gamma)} T_{k+\gamma}(z)
\end{array}
\right\} \tag{40}
$$

Similarly to the two-dimensional case, we need the superposition of five polynomials in each spatial direction. The substitution of (39,40) in the boundary conditions defines a set of linear equations for the coefficients $\tilde{f}_{i\alpha}$, $\hat{f}_{i\alpha}$, $\tilde{g}_{j\beta}$, $\hat{g}_{j\beta}$, $\tilde{h}_{k\gamma}$, $\hat{h}_{k\gamma}$.

2.2.5   Basis functions for a three-dimensional divergence-free vector field in cylindrical coordinates

Obviously, in the case of a curvilinear system of coordinates the divergent-free basis functions must be defined in a different way. In the following we describe the basis functions for the cylindrical coordinates, which were successfully used in [3], [4], and [9].

Consider a problem defined in a cylinder, $0 \le r \le 1, \quad 0 \le z \le A, \ 0 \le \varphi \le 2\pi$. Using the 2π-periodicity in the φ-direction, the solution can be expressed as a classical trigonometric Fourier series

$$
\mathbf{v} = \sum_{k=-\infty}^{k=\infty} \mathbf{v}_k(r,z) exp(ik\varphi) \tag{41}
$$

It follows from the divergence-free requirement

$$
\nabla \cdot \mathbf{v} = \frac{\partial v^{(r)}}{\partial r} + \frac{v^{(r)}}{r} + \frac{1}{r}\frac{\partial v^{(\varphi)}}{\partial \varphi} + \frac{\partial v^{(z)}}{\partial z} = \frac{\partial v^{(r)}}{\partial r} + \frac{v^{(r)}}{r} + \frac{ik}{r}v^{(\varphi)} + \frac{\partial v^{(z)}}{\partial z} = 0 \tag{42}
$$

11

that one has to distinguish between the mode $k = 0$ (i.e., axisymmetric case, no requirements on $v^{(\varphi)}$) and the modes $k \neq 0$. In other words, the axisymmetric part of the flow ($k = 0$) must be treated separately from the purely non-axisymmetric part ($k \neq 0$). Thus the field $\mathbf{v}$ should be represented as

$$\mathbf{v} = \sum_{i=1}^{M_r} \sum_{j=1}^{M_z} A_{ij} \mathbf{U}_{ij}(r,z) + \sum_{k=-\infty}^{k=\infty} \left\{ \sum_{i=1}^{N_r} \sum_{j=1}^{N_z} \left[B_{ij}^k \mathbf{V}_{ij}(r,z) + C_{ij}^k \mathbf{W}_{ij}(r,z) \right] \right\} exp(ik\varphi) \quad (43)$$

where the vector functions $\mathbf{U}_{ij}$ form the basis of the axisymmetric part ($k=0$) of the 3D flow in the (r,z) plane, the vector functions $\mathbf{V}_{ij}$ and $\mathbf{W}_{ij}$ form bases for the remaining part of the three-dimensional flow in the $(r\text{-}\varphi)$ and $(z\text{-}\varphi)$ coordinate surfaces respectively, and A_{ij}, B_{ij}^k and C_{ij}^k are unknown coefficients. Similarly to the bases in the Cartesian coordinates, the components of basis functions, that are normal to the corresponding coordinate surfaces vanish: $U_{ij}^{(\varphi)} = V_{ij}^{(z)} = W_{ij}^{(r)} = 0$.

The scalar components of the basis functions $\mathbf{U}_{ij}$, $\mathbf{V}_{ij}$ and $\mathbf{W}_{ij}$ are defined on the basis of the Chebyshev polynomials as:

$$\mathbf{U}_{ij} = \begin{bmatrix} \dfrac{r}{2} \sum_{l=0}^{4} a_{il} T_{i+l}(r) \sum_{m=0}^{4} b_{jm} U_{j+m-1}\left(\dfrac{z}{A}\right) \\[2ex] 0 \\[2ex] -\dfrac{A}{2} \sum_{l=0}^{4} a_{il} \tilde{U}_{i+l-1}(r) \sum_{m=0}^{4} \dfrac{b_{jm}}{(j+m)} T_{j+m}\left(\dfrac{z}{A}\right) \end{bmatrix}$$

$$(44)$$

$$\mathbf{V}_{ij} = \begin{bmatrix} -ikr^{\alpha} \sum_{l=0}^{4} c_{il} T_{i+l}(r) \sum_{m=0}^{4} d_{jm} T_{j+m}\left(\dfrac{z}{A}\right) \\[2ex] \sum_{l=0}^{4} c_{il} \hat{U}_{i+l}(r) \sum_{m=0}^{4} d_{jm} T_{j+m}\left(\dfrac{z}{A}\right) \\[2ex] 0 \end{bmatrix} \quad (45)$$

$$\mathbf{W}_{ij} = \begin{bmatrix} 0 \\[2mm] r^2 \sum\limits_{l=0}^{4} e_{il} T_{i+l}(r) \sum\limits_{m=0}^{4} f_{jm} U_{j+m-1}\left(\dfrac{z}{A}\right) \\[4mm] -\dfrac{ikA}{2} r \sum\limits_{l=0}^{4} e_{il} T_{i+l}(r) \sum\limits_{m=0}^{4} \dfrac{f_{jm}}{(j+m)} T_{j+m}\left(\dfrac{z}{A}\right) \end{bmatrix} \tag{46}$$

Here *a=0* for *|k|=1* and *a=1* for *|k|>1*, and

$$\tilde{U}_n(r) = T_{n+1}(r) + (n+1)rU_n(r), \qquad \hat{U}_n(r) = (\alpha+1)r^\alpha T_n(r) + 2nr^{\alpha+1}U_{n-1}(r) \tag{47}$$

The coefficients a_{il}, b_{jm}, c_{il}, d_{jm}, e_{il}, f_{jml} are used to satisfy all the boundary conditions. As previously, eq.(42) follows from the relation (12).

2.2.6   Application to the Navier-Stokes and transport equations

Consider an incompressible flow defined by the equations of momentum and continuity, as well as by the transport of a scalar property θ (e.g., θ is the temperature):

$$\frac{\partial \mathbf{v}}{\partial t} + (\mathbf{v} \cdot \nabla)\mathbf{v} = -\nabla p + \frac{1}{Re}\Delta \mathbf{v} + \mathbf{f} \tag{48.1}$$

$$\nabla \cdot \mathbf{v} = 0 \tag{48.2}$$

$$\frac{\partial \theta}{\partial t} + (\mathbf{v} \cdot \nabla)\theta = \frac{1}{Pe}\Delta\theta + q \tag{48.3}$$

where $\mathbf{v}$ is the fluid velocity, p is pressure, $\mathbf{f}$ is volume force, q is a volume source of θ, and *Re* and *Pe* are the Reynolds and Peclet number.

The use of the global spectral approach gives some additional advantages. When there is no flow through the boundaries of the flow region ($\mathbf{v} \cdot \mathbf{n}|_\Gamma = 0$) the pressure gradient is orthogonal to the divergence-free velocity field (Ω is the flow region and Γ is its boundary):

$$\langle \mathbf{v}, \nabla p \rangle = \int_\Omega \mathbf{v} \cdot \nabla p \, d\Omega = \int_\Omega \nabla \cdot (\mathbf{v}p) \, d\Omega - \int_\Omega p \nabla \cdot \mathbf{v} \, d\Omega = \int_\Omega \nabla \cdot (\mathbf{v}p) \, d\Omega = \int_\Gamma \mathbf{v} \cdot \mathbf{n} \, d\Gamma = 0 \tag{49}$$

Obviously, (49) holds if **v** is replaced by a divergent-free basis function satisfying the no-through flow boundary conditions, i.e., a basis function from (39), (40) or (44)-(46). Therefore, the implementation of a weighted residuals method with a proper projection system excludes the pressure from the numerical model.

We further assume that the velocity is approximated by a series

$$\mathbf{v} = \sum_{i=0}^{N} X_i(t)\, \mathbf{j}_i(\mathbf{r}) \tag{50}$$

Here **r** is the radius-vector of a point in the flow region, $X_i(t)$ are unknown time-dependent coefficients and $\mathbf{j}_i$ are the basis functions. It is supposed that the multiple indices of decompositions like (38) and (43) are reordered into a single index i (for details see [2],[3]). Suppose also that the classical Galerkin method is applied ,i.e., $\{\mathbf{j}_i\}$ serves as both the trial and the weight system. Then the Galerkin procedure reduces (48) to an ODE system, which can be written as

$$\tilde{S}_{ij}\dot{X}_i = \tilde{S}_{ij}\frac{dX_i(t)}{dt} = \tilde{F}_i(\mathbf{X}(t),\mu) = \tilde{L}_{ij}X_j + \tilde{N}_{ijk}X_jX_k + \tilde{Q}_i \tag{51}$$

The matrices $\tilde{L}_{ij}, \tilde{N}_{ijk}, \tilde{Q}_i$ contain coefficients of linear, bilinear and free terms of (48), respectively. It is assumed that these matrices depend on a control parameter μ ($\mu = Re$ in case of eq.(48.1)). The ODE system (51) corresponds to the case of a parabolic polynomial non-linearity of the considered problem. In the case of polynomial non-linearity of higher degree there will be additional terms described by matrices of higher dimension. In the case of non-polynomial non-linearity the additional terms will contain more complicated functions of X_i. However, this will cause only technical changes in the implementation of the method described below.

The use of the divergent-free basis functions, which satisfy the boundary conditions lead to several definite properties of the matrices in (51). Thus, the conservation laws

$$\langle(\mathbf{v}\cdot\nabla)\mathbf{v},\mathbf{v}\rangle = 0 \qquad \text{and} \qquad \langle(\mathbf{v}\cdot\nabla)\theta,\theta\rangle = 0 \tag{52}$$

lead to the relation

$$\tilde{N}_{ijk}X_iX_jX_k = 0 \tag{53}$$

for any vector **X**. The well-known Green's theorems

$$\langle\Delta\mathbf{v},\mathbf{v}\rangle = -\langle\nabla\times\mathbf{v},\nabla\times\mathbf{v}\rangle \qquad \text{and} \qquad \langle\Delta\theta,\theta\rangle = -\langle\nabla\theta,\nabla\theta\rangle \tag{54}$$

lead to the symmetry of the matrices corresponding to the projections of the Laplacian operators. Furthermore, these matrices are negatively defined like the Laplacian operators. The described properties, especially (53), can be used as preliminary tests in the programming of the method.

The Gram matrix $\widetilde{S}_{ij} = \langle \mathbf{j}_i, \mathbf{j}_j \rangle \neq I$ (I is the identity matrix) arises because the basis functions are not orthonormal. Multiplication of the left and the right hand sides of (51) by the inverse matrix $\widetilde{S}_{ij}^{-1}$ reduces the dynamical system to the following explicit form:

$$\dot{X}_i = \frac{\mathrm{d}X_i(t)}{\mathrm{d}t} = F_i(\mathbf{X}(t), \mu) = L_{ij}X_j + N_{ijk}X_jX_k + Q_i \tag{55}$$

The calculation of the inverse matrix $\widetilde{S}_{ij}^{-1}$ usually does not cause any numerical difficulties. The explicit form of the ODE system (55) allows one to use standard numerical methods, developed for ODEs and systems of non-linear algebraic equations, to obtain stationary and non-stationary solutions and for the investigation of the stability of these solutions. For example, a steady solution of (55) can be calculated by Newton iteration. In the case of multiple solutions the arc-length continuation technique can be implemented to follow a certain solution path.

Assume that $\mathbf{X} = \mathbf{X}^0$ is a steady solution of (55). The linear stability of solution $\mathbf{X}^0$ is defined by the eigenvalues of the Jacobian matrix

$$J_{mk} = \frac{\partial \dot{X}_m}{\partial X_k} = L_{mk} + (N_{mkn} + N_{mnk})X_n^0 \tag{56}$$

The steady solution $\mathbf{X} = \mathbf{X}^0$ is unstable if there exists at least one eigenvalue of J_{mk} with a positive real part. The study of stability requires to determine a value of the governing parameter μ such that the real part of the dominant eigenvalue (eigenvalue with the maximal real part) $L = L^r + iL^i$ is zero: $L^r = 0$ and $\P L^r / \partial \mu \neq 0$. If $L^i = 0$ then a bifurcation from one steady solution to another can be expected. If $L^i \neq 0$ then a bifurcation to a periodic solution (Hopf bifurcation) takes place. In the latter case $w_{cr} = L^i$ estimates the circular frequency of the oscillatory solution which branches from the steady state after the onset of the oscillatory instability. The most unstable perturbation of the dynamical system (55) is defined by the eigenvector $\mathbf{V}$ corresponding to the dominant eigenvalue Λ with $L^r = 0$ ($J_{mk}V_k = LV_m = iL^iV_m$). Components of the eigenvector $\mathbf{V}$, redefined as the coefficients X_i from (50), define the expansion of the most unstable perturbation of the flow in the Galerkin series (50). Similarly, the limit cycle of the dynamical system (55), which

develops as a result of Hopf bifurcation, defines an approximation of the periodic solution of the considered problem.

The computational process should be arranged in the following way: first, for an initial value of the control parameter μ^0 a stationary solution of ODE system (55) is calculated; then the eigenvalues of the Jacobian matrix (56) are computed (in [2]-[10] the QR decomposition algorithm was used). These two steps are repeated for the next value of the control parameter $\mu^1 > \mu^0$. Then the real part of the dominant eigenvalue L^r is considered as a function of μ, and the critical value is calculated as a solution of the equation $L^r(\mu_{cr}) = 0$ (in [2]-[10] it was solved by the secant method). If at $m = m_r$ a Hopf bifurcation takes place then the branching oscillatory state may be asymptotically approximated as [12]

$$\mu = \mu_{cr} + \mu_1 \varepsilon^2 + O\!\left(\varepsilon^4\right) \tag{57.1}$$

$$\tau(\mu) = \frac{2\pi}{\omega_{cr}}\left[1 + \tau_1 \varepsilon^2 + O\!\left(\varepsilon^4\right)\right] \tag{57.2}$$

$$\mathbf{X}(t;\mu) = \mathbf{X}^0(\mu_{cr}) + \varepsilon\, Real\!\left[\mathbf{V}\, exp\!\left(\frac{2\pi i}{\tau}t\right)\right] + O\!\left(\varepsilon^2\right) \tag{57.3}$$

Here ε is a formal positive parameter, $(\mu-\mu_{cr})$ is the supercriticality, w_{cr} is the critical circular frequency, τ is the period of oscillations, and $\mathbf{X}$ is the asymptotic oscillatory solution of the ODE system (55) for the control parameter defined in (57a). The asymptotic expansion (57) is defined by two parameters μ_1 and τ_1, which are calculated using the algorithm of [12]. This algorithm, as well as its implementation for the described dynamical system, is briefly described below. The parameters μ_1 and τ_1 are defined by

$$\mu_1 = -\frac{Real(\sigma)}{\alpha^r}, \qquad \tau_1 = -\frac{1}{\omega_{cr}}\left[Im(\sigma) + \mu_1 \alpha^i\right] \tag{58}$$

where α is the derivative of the dominant eigenvalue with respect to the control parameter

$$\alpha = \alpha^r + \alpha^i = \left.\frac{d\Lambda}{d\mu}\right|_{\mu=\mu_{cr}} \tag{59}$$

and the complex number σ can be obtained via the following algorithm (here $\mathbf{F}$ is the right hand side of the dynamical system, $\mathbf{X}^0$ is steady solution in the critical point, $\mathbf{U}$ and $\mathbf{V}$ are the left and right eigenvectors of the Jacobian matrix $\mathbf{J}$, and ς is a complex number):

$$\sigma = \frac{1}{2}G_{21} + \frac{1}{2\omega_0}\left[g_{20}g_{11} - 2|g_{11}|^2 - \frac{1}{3}|g_{02}|^2 \right] \tag{60}$$

$$g_{20} = 2\mathbf{U}^{\mathsf{T}}\mathbf{f_{20}}, \qquad g_{02} = 2\mathbf{U}^{\mathsf{T}}\bar{\mathbf{f}}_{20}, \qquad\qquad g_{11} = 2\mathbf{U}^{\mathsf{T}}\mathbf{f}_{11} \tag{61}$$

$$\mathbf{f_{20}} = \left.\frac{\partial^2}{\partial\varsigma^2}\mathbf{F}\left[\mathbf{X^0} + Real(\mathbf{V}\varsigma); \mu_{cr}\right]\right|_{\varsigma=0}, \qquad \mathbf{f}_{11} = \left.\frac{\partial^2}{\partial\varsigma\partial\bar\varsigma}\mathbf{F}\left[\mathbf{X^0} + Real(\mathbf{V}\varsigma); \mu_{cr}\right]\right|_{\varsigma=0} \tag{62}$$

$$G_{21} = \left.\frac{\partial^3}{\partial\varsigma^2\partial\bar\varsigma}\left\{ 2\mathbf{U}^{\mathsf{T}}\mathbf{F}\left[\mathbf{X^0} + Real\left(\mathbf{V}\varsigma + \mathbf{w}_{20}\varsigma^2 + \mathbf{w}_{11}\varsigma\bar\varsigma\right); \mu_{cr}\right]\right\}\right|_{\varsigma=0} \tag{63}$$

and the vectors $\mathbf{w}_{11}$ and $\mathbf{w}_{20}$ are solutions of the following linear algebraic systems:

$$\mathbf{Jw_{11}} = -\mathbf{h}_{11}, \quad \left[\mathbf{J} - 2i\omega_0\mathbf{I}\right]\mathbf{w_{20}} = -\mathbf{h_{20}}, \qquad \mathbf{h_{ij}} = \left[\mathbf{I} - 2\,Real\left(\mathbf{VU}^{\mathsf{T}}\right)\right]\mathbf{f_{ij}}. \tag{64}$$

The most difficult part of the implementation of this algorithm is the calculation of the second (62) and the third (63) derivatives of the right hand side of the ODE system. The number of the ODEs usually reaches several thousands and numerical differentiation can lead to unacceptably large errors. However, the explicit form of (55) allows analytical calculation of (62) and (63). In the case of parabolic non-linearity this yields:

$$f_{20,k} = \frac{1}{2}\left[N_{kij}\left(V_i^{(r)}V_j^{(r)} - V_i^{(i)}V_j^{(i)}\right) + iN_{kij}\left(V_i^{(r)}V_j^{(i)} - V_i^{(i)}V_j^{(r)}\right) \right] \tag{65}$$

$$f_{11,k} = \frac{1}{2}N_{kij}\left(V_i^{(r)}V_j^{(r)} + V_i^{(i)}V_j^{(i)}\right) \tag{66}$$

$$G_{21} = \frac{1}{2}U_i\left(N_{ijm} + N_{imj}\right)\left[2w_{11,j}V_m + w_{20,j}\bar{V}_m\right] \tag{67}$$

The use of (65)-(67) allows one to compute the asymptotic expansions (57) without significant loss of accuracy. The CPU-time requirements for such calculations are comparable with the calculation of a single steady state solution. Note, that the sign of μ_1 defines whether the bifurcation is sub- or super-critical.

3   EXAMPLES OF APPLICATIONS

As was stated above, the main goal of the described approach is to reduce the number of degrees of freedom of the numerical model. Several benchmark problems were solved to validate the approach and to study the convergence.   Furthermore, we made detailed comparisons with the results of our own finite volume solver. Details on various test calculations can be found in [2]-[8]. The accumulated experience shows that our approach really allows one to reduce the number of degrees of freedom. We estimate that the accuracy of 100×100 to 200×200 finite volume grid can be reached with the use of 30×30 to 40×40 basis functions of the global Galerkin method. Such a significant reduction of the number of degrees of freedom allowed us to perform parametric studies of linear stability of various fluid flows.

The main result of each stability study is diagrams showing the dependence of critical parameters on other governing parameters of the problem. Two examples are shown in Figs.1 and 2. Figure 1 corresponds to the onset of the oscillatory instability of convective flow in a laterally heated square cavity (details can be found in [8]). It is seen that the neutral curve $Gr_{cr}(Pr)$ is non-monotonous and contains breaks and hysteresis loops. Clearly, such a complicated neutral curve cannot be obtained by a straight-forward time-integration of the governing equations. The change of the pattern of the convective flow along the neutral curve is illustrated as insets in Fig.1a. Each inset in Fig.1a contains the streamlines (left frame) and the isotherms (right frame) at the critical point shown. Breaks of the neutral curve $Gr_{cr}(Pr)$ correspond to the change of the most dangerous perturbation (described by the eigenvector of the linear stability problem) of the flow. Each break of the neutral curve $Gr_{cr}(Pr)$ is followed by an abrupt change of the critical frequency (different eigenvectors correspond to different eigenvalues whose imaginary part is the critical circular frequency, see above). Patterns of the most dangerous perturbation are illustrated in the insets of Fig.1b (left frames correspond to perturbation of the stream function, right frames – to perturbation of the temperature). According to the linear stability theory the perturbations are defined to within multiplication by a constant, and their isolines coincide with the isolines of the amplitude of oscillations in the supercritical state (for details see [2] and [3]). Note, that the stability diagram, shown in Fig.1, is drawn through several tens of calculated critical points. Sometimes it is necessary to calculate several hundreds of critical points to complete the stability diagrams [4], [8]. Especially difficult are cases where multiple stable steady states exist, and the stability of each branch of steady state has to be studied separately [8]. It should be noted, that the knowledge of the existence

of the multiplicity and possibility of path-following (both provided by the described approach) allowed us to explain some experimental results which had no satisfactory theoretical explanation before [7],[8].

The abrupt changes of the most dangerous perturbation were observed in all parametric studies reported in [3]-[10]. Figure 2, corresponding to the oscillatory instability of a swirling flow in a cylinder whose top and bottom corotate with the same angular velocity [5], provides an additional example of such abrupt changes. Patterns of the flow are included as insets in Fig.2a (left frame – isolines of the azimuthal velocity, right frames – streamlines of the meridional flow). Patterns of the corresponding most dangerous perturbation are shown as insets in Fig.2b (left frame – perturbation of the azimuthal velocity, right frames – perturbation of the meridional stream function). All the insets show only the upper half of a cylinder, since the flow and the perturbation are symmetric with respect to the midplane. The patterns of the flow are similar for all aspect ratios, and can be characterized by two strong meridional vortices and a weak recirculation zone containing a double vortex ring. Patterns of the perturbation, however, differ at different branches of the neutral curves. On the other hand, different perturbation patterns have one common feature – a global maximum of the azimuthal velocity perturbation is located in the middle of the recirculation zone. Therefore, it can be assumed that in all cases the instability sets in inside the recirculation zone, but results in different oscillatory flow patterns at different values of the aspect ratio.

An example of the asymptotic approximation of the oscillatory solution (57) is shown in Fig.3. Supercritical oscillatory convective flow in a laterally heated cavity is considered [7]. Here the asymptotic approximation of oscillatory convective flow, calculated with 30×30 basis functions, is compared with the solution of the full unsteady problem on a 100×100 finite volume grid. It is seen that results are very close, such that no heavy time-dependent calculations are needed to obtain the correct pattern of oscillatory solution at not very large supercriticalities.

Another advantage of the global spectral approach is the analytical representation of the approximate solution over the whole domain. This allows an easy analytical calculation of derivatives and integrals of the solution, as was done in [2] for the calculation of the Nusselt number, and in [3] for the calculation of vorticity. This advantage is illustrated also in the next example (Fig.4), where the trajectories of tracers, immersed in a liquid for visualization of the flow, are calculated using the velocity approximated by series (50) and therefore defined at each point of the flow region. For the considered problem of the swirling flow in a cylinder with rotating lid [3] the latter requires solution of the following ODE system:

$$\frac{dr}{dt} = v^{(r)} + f_{cent}$$

$$r\frac{d\varphi}{dt} = v^{(\varphi)} + f_{cor} \qquad (68)$$

$$\frac{dz}{dt} = v^{(z)} + f_b$$

where f_{cent}, f_{cor} and f_b are the centrifugal, Coriolis and buoyancy forces respectively, which arise due to a slight difference of the liquid and tracer densities. Solution of (68) requires the calculation of the velocity at an arbitrary point (r,φ,z) and is extremely sensitive to numerical errors. The analytical approximation, provided by a global spectral method, allows one to calculate the velocity as a summation of the corresponding series, without introducing an additional numerical error. The trajectories shown in Fig.3 are calculated using the steady axisymmetric velocity field. The non-axisymmetric pattern of the trajectories is caused by the already mentioned density difference (2% difference is enough to cause this effect). Such non-axisymmetric trajectories, observed in experiment, were mistakenly interpreted as the result of a non-axisymmetric flow [13].

4 CONCLUDING REMARKS

The proposed approach was used for the study of stability of swirling flows [3]-[5], buoyancy-driven convection [6]-[8],[10], and axisymmetry-breaking bifurcations of convective flows [9]. In all these problems fast convergence of the Galerkin method allowed us to complete the stability analysis for wide ranges of the governing parameters. The stability diagrams obtained show regions of stability and possible multiplicity of steady state solutions. A relatively small number of degrees of freedom allowed us also to perform a weakly nonlinear analysis of slightly supercritical oscillatory states and to obtain the asymptotic approximation of the oscillatory states without solution of the full unsteady problem [3],[6],[7]. The approach was easily extended for the study of axisymmetry-breaking three-dimensional instabilities [9] and to fully three-dimensional stability problems [10].

The main restriction of the described approach is that the shape of the flow region should be a canonical domain. Apparently, an extension to flow regions of more complicated shape should include a transformation of the domain or combination of the described approach with the finite element or spectral element formulation. It can cause some additional numerical difficulties connected with the calculation of the inner products of the basis functions. The inner products of the

polynomial basis functions in [2]-[10] were calculated analytically. In the case of more complicated flow regions this will be hardly possible. On the other hand, recent results of [14] (where a similar Galerkin approach was used) show that numerical evaluation of the inner products also can lead to sufficiently good results.

Acknowledgments

REFERENCES

[1]   W.S. Edwards, L.S. Tuckerman, R.A.Friesner, and D.C.Sorensen (1994) Krylov methods for the incompressible Navier-Stokes equations. Journal of Computational Physics, vol.110, pp.82-102

[2]   A.Yu. Gelfgat and I. Tanasawa (1994) Numerical analysis of oscillatory instability of buoyancy convection with the Galerkin spectral method. Numerical Heat Transfer. Part A: Applications, vol.25, pp.627-648

[3]   A.Yu. Gelfgat A., P.Z. Bar-Yoseph, and A. Solan (1996) Stability of confined swirling flow with and without vortex breakdown. Journal of Fluid Mechanics, vol.311, pp.1-36

[4]   A.Yu. Gelfgat, P.Z. Bar-Yoseph and A. Solan (1996) Vortex breakdown and instability of swirling flow in a cylinder with rotating top and bottom. Physics of Fluids, vol.8, pp.2614-2625

[5]   A.Yu. Gelfgat, P.Z. Bar-Yoseph and A. Solan (1996) Confined Swirling Flow Simulation Using Spectral Galerkin and Finite Volume Methods. *Proc. 1996 ASME Fluids Engineering Division Conference*, San-Diego, CA, July 7-11, 1996, vol.3, FED, vol.238, pp.105-111.

[6]   A.Yu. Gelfgat, P.Z. Bar-Yoseph, and A.L. Yarin (1997) On oscillatory instability of convective flows at low Prandtl number. Journal of Fluids Engineering, vol.119, pp.823-830

[7]   A.Yu. Gelfgat, P.Z. Bar-Yoseph, and A.L. Yarin (1999) Non-symmetric convective flows in laterally heated rectangular cavities. Int. J. Computational Fluid Dynamics, vol.11, pp.261-273

[8]   A.Yu. Gelfgat, P.Z. Bar-Yoseph, and A.L. Yarin (1999)   Stability of multiple steady states of convection in laterally heated cavities. Journal of Fluid Mechanics, vol.388, pp.315-334.

[9]   A.Yu. Gelfgat, P.Z. Bar-Yoseph, A.Solan, and T.A. Kowalewski (1999) An axisymmetry-breaking instability of axially symmetric natural convection. Int. J. Transport Phenomena (to appear).

[10]   A.Yu. Gelfgat (1999) Different modes of Rayleigh-Benard instability in two- and three-dimensional rectangular enclosures (submitted).

[11]   A.Zebib (1984) A Chebyshev method for the solution of boundary value problems. Journal of Computational Physics, vol.53, pp.443-455.

[12]   B.D.Hassard, N.D.Kazarinoff and Y.-H.Wan (1981*) Theory and Applications of Hopf Bifurcation*. London, Math. Soc. Lecture Note Series, vol.41.

[13]   A.Spohn, M.Mory and E.J.Hopfinger (1998) Experiments on vortex breakdown in a confined flow generated by a rotating disc. Journal of Fluid Mechanics, vol.370, pp.73-99.

[14]   H.Yahata (1999) Stability analysis of natural convection in vertical cavities with lateral heating. Journal of Physical Society of Japan, vol.68, pp.446-460.

FIGURE CAPTIONS

Fig.1. Convection in a laterally heated square cavity. Dependence of the critical Grashof number (a) and the critical circular frequency (b) on the Prandtl number. Insets: streamlines and isotherms at critical points (a); isolines of perturbations of the stream function and the temperature (b).

Fig.2. Swirling flow in a cylinder with corotating top and bottom. Dependence of the critical Reynolds number (a) and the critical circular frequency (b) on the aspect ratio. Insets: streamlines and isolines of the azimuthal velocity at critical points (a); isolines of perturbations of the stream function and the azimuthal velocity (b).

Fig.3. Convection in a laterally heated square cavity. Instantaneous streamlines of a convective flow plotted for equal time intervals covering the complete period. $Pr = 0$, $Gr = 4.5 \times 10^5$ (for details see [7]). Left frames – asymptotic approximation (57) using 30×30 basis functions, right frames – time-dependent calculation using 100×100 finite volume grid.

Fig.4. Swirling flow in a cylinder with rotating lid. Trajectories of visualization tracers crossing the plane $\varphi = 0, \pi$. Calculation is based on steady axisymmetric solution obtained with 30×30 basis functions.
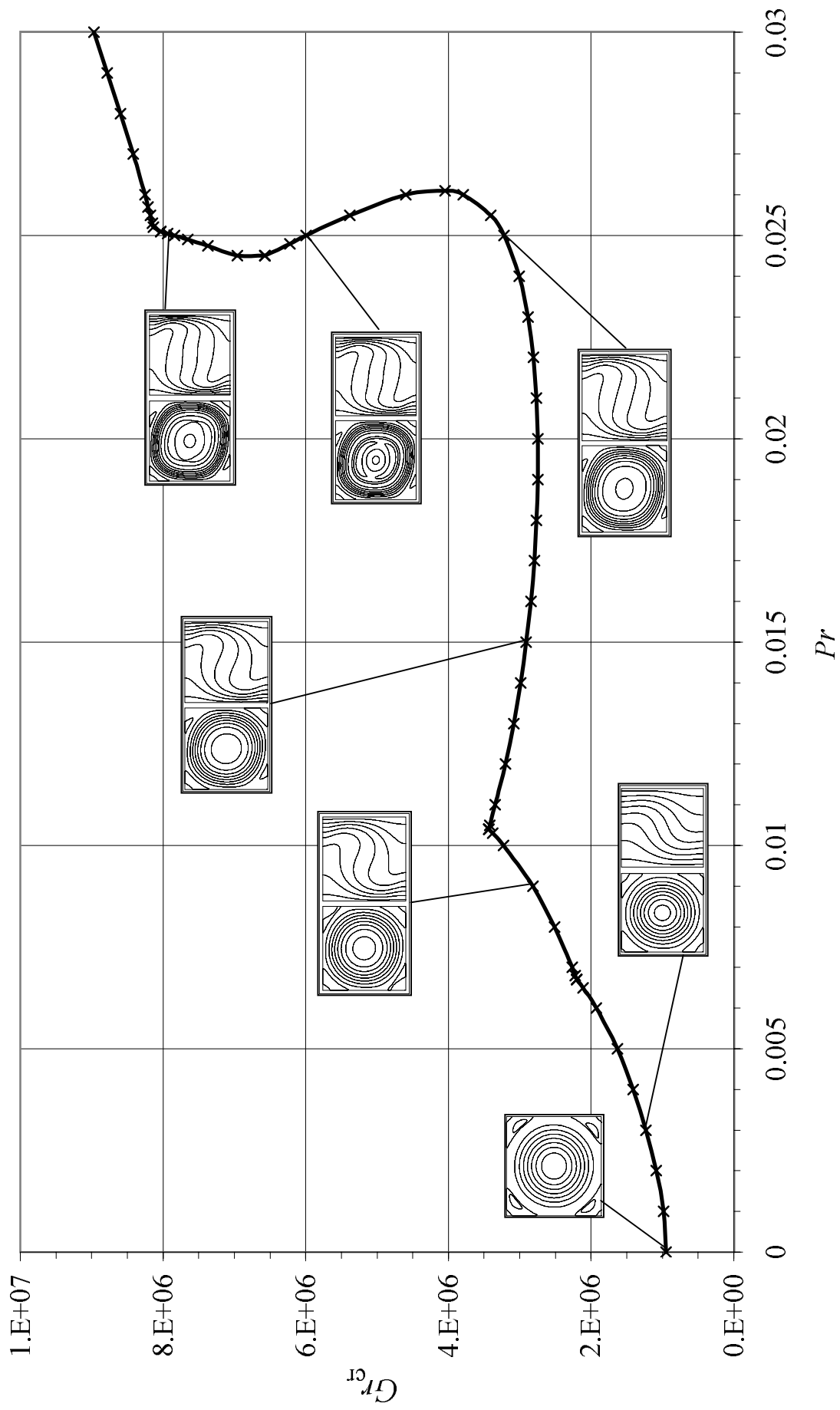
Fig 1a. Convection in a laterally heated square cavity. Dependence of the critical Grashof number on the Prandtl number. Insets: streamlines and isotherms at critical points.
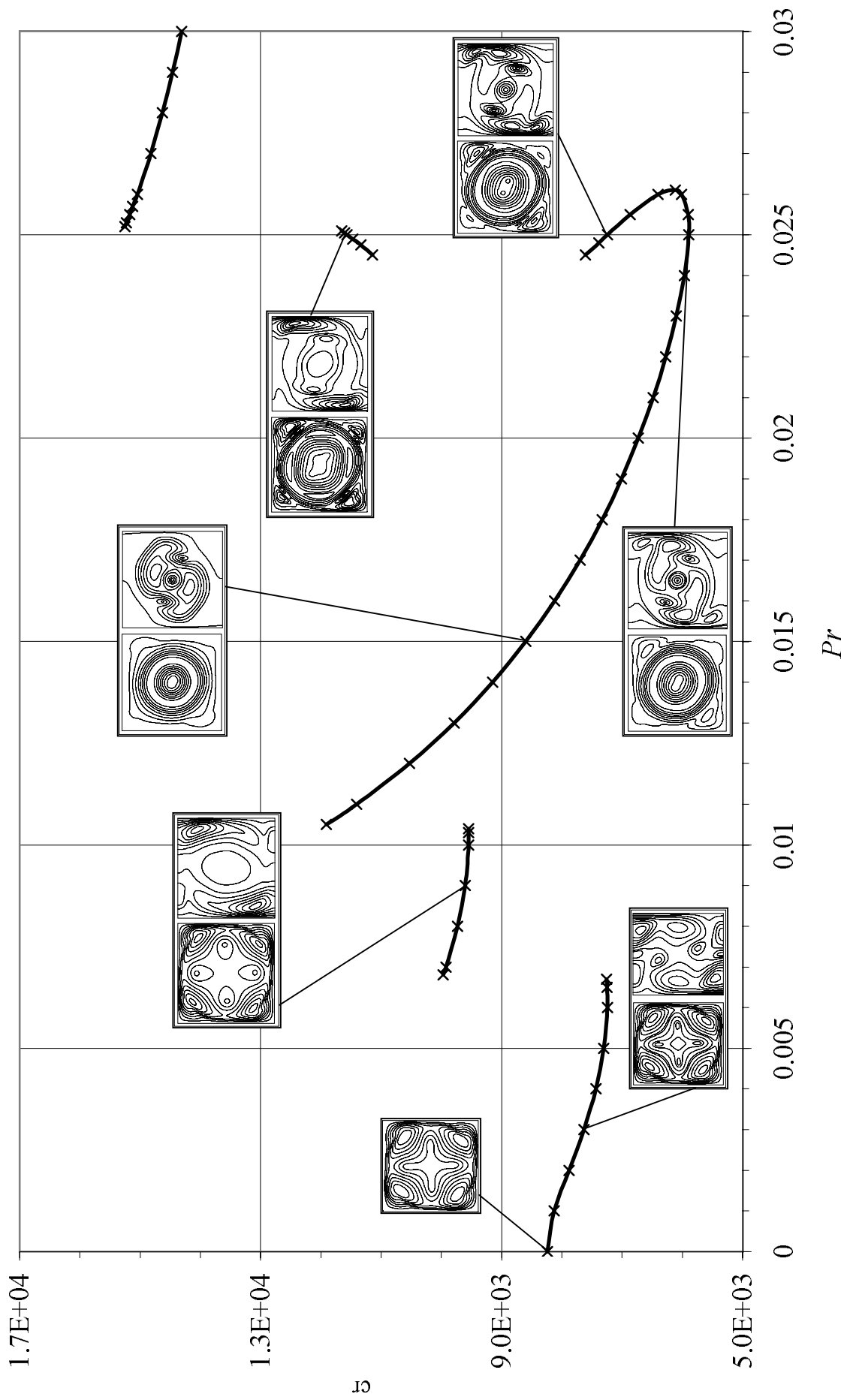
Fig.1b. Convection in a laterally heated suare cavity. Dependence of the critical circular frequency on the Prandtl number. Insets: isolines of perturbations of the stream function and the temperature.
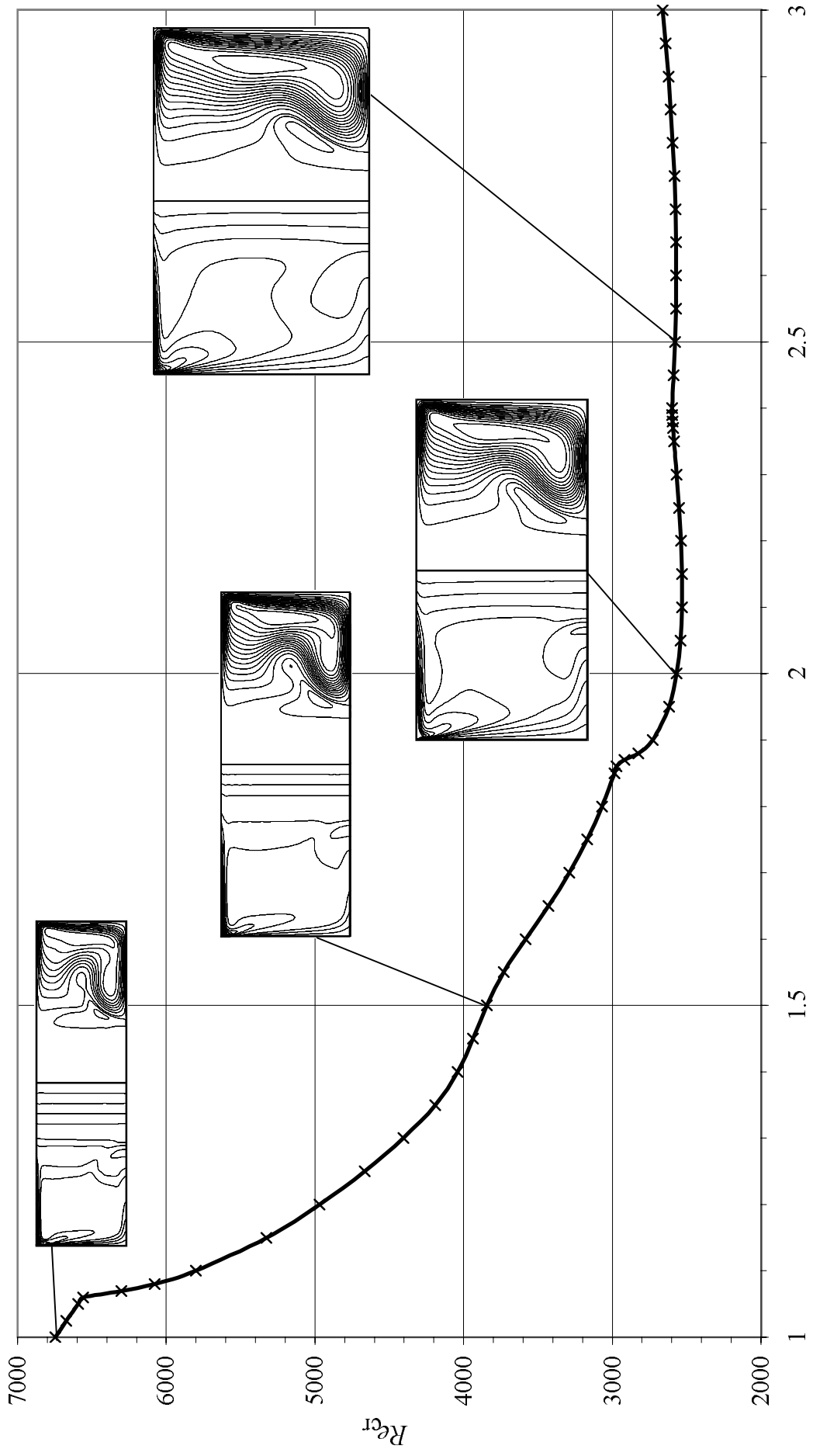
Fig.2a. Swirling flow in a cylinder with corotating top and bottom. Dependence of the critical Reynolds number on the aspect ratio. Insets:streamlines and isolines of the azimuthal velocity at critical points.
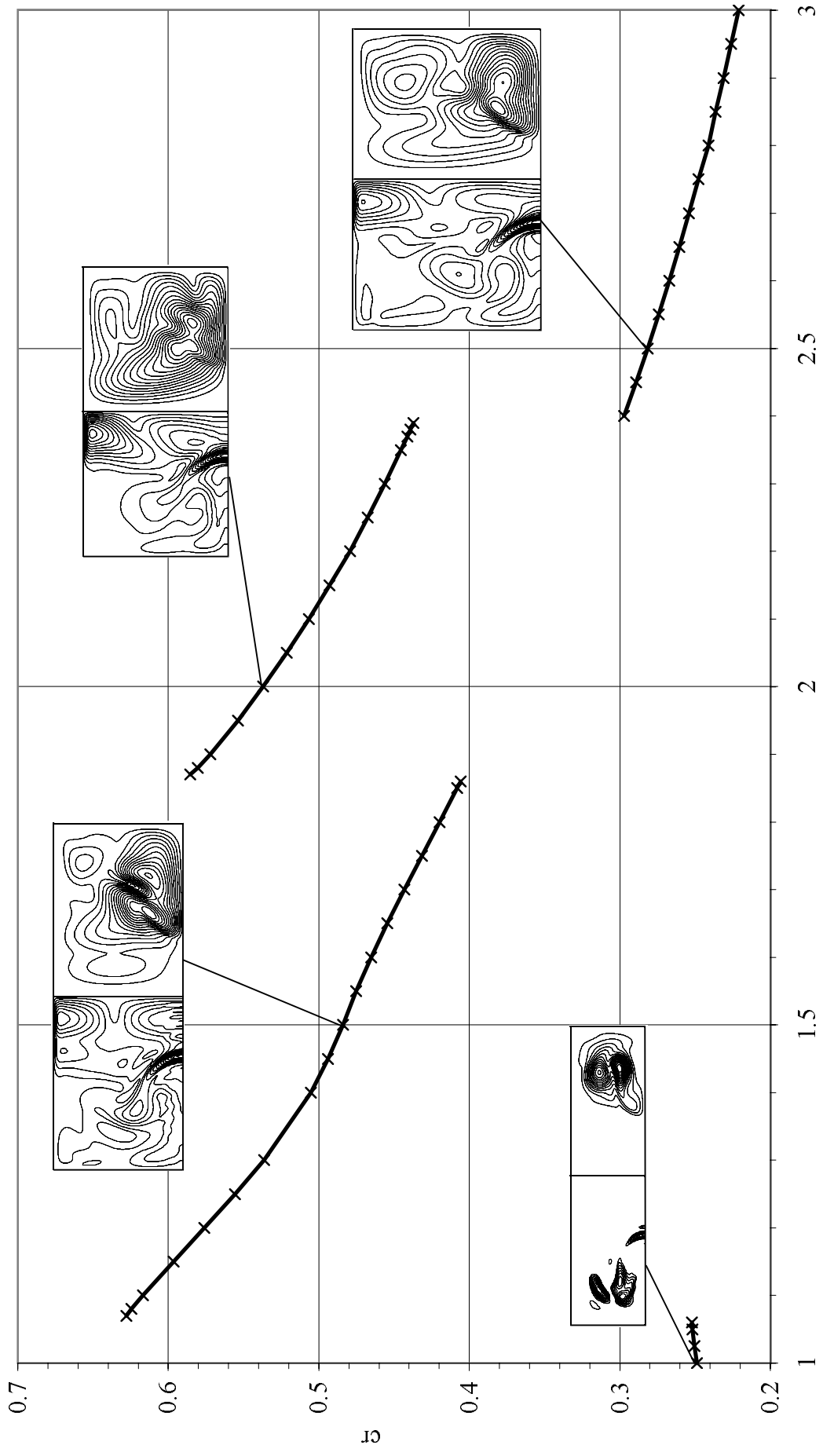
Fig.2b. Swirling flow in a cylinder with corotating top and bottom. Dependence of the critical circular frequency on the aspect ratio. Insets: isolines of perturbations of the stream function and the azimuthal velocity.
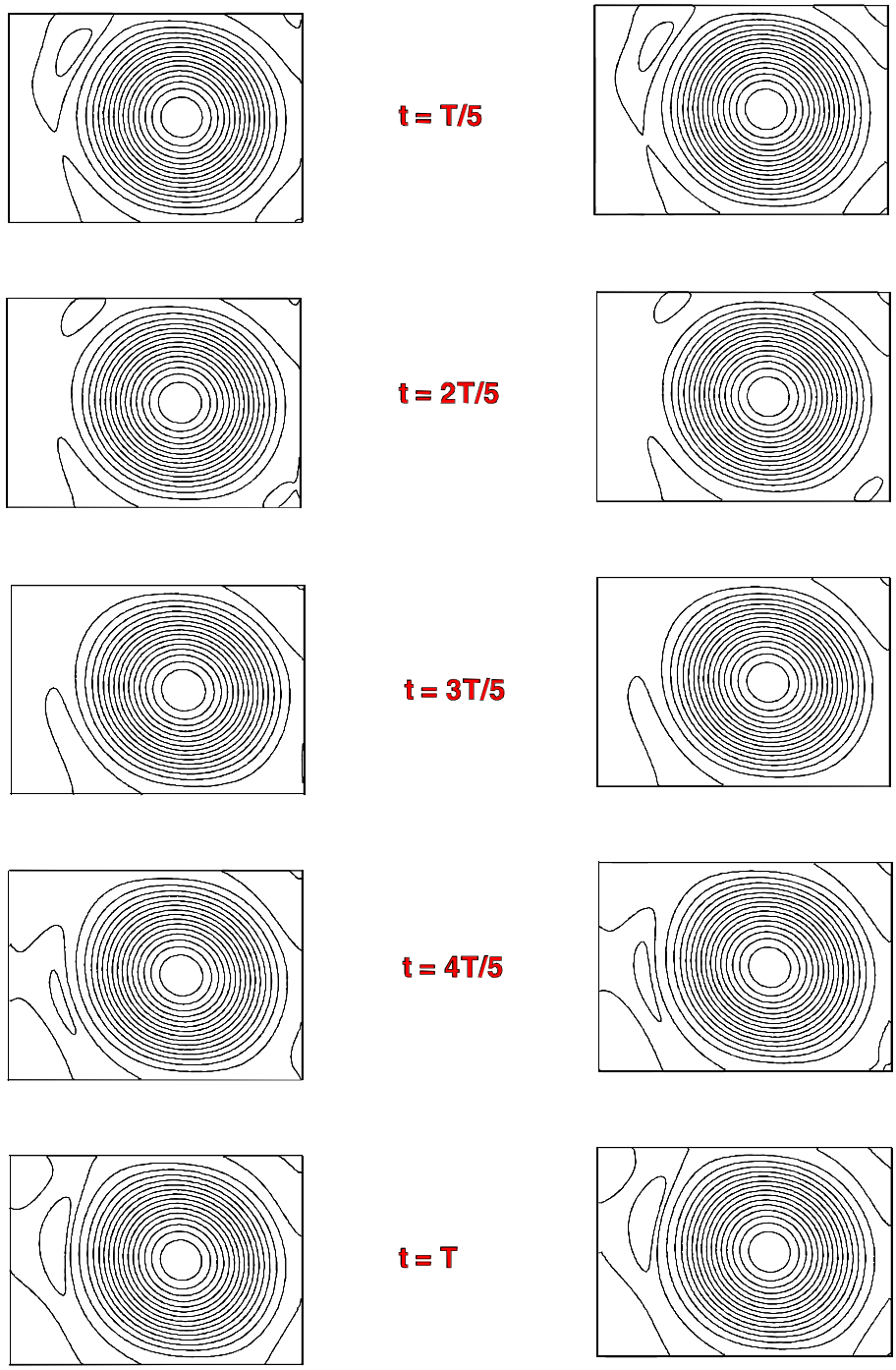
Fig.3. Convection in a laterally heted cavity. Instantenous streamlines plotted for equal time intervals covering the complete period. Pr=0, A=1.4, Gr=450,000 (for details see [7]). Left frames - asymptotic approximation (57) using 30x30 basis functions, right frames - time-dependent calculation using 100x100 finite volume grid.

Fig.4. Flow in a cylinder with rotating lid. Trajectories of visualization tracers crossing the plane φ=0,π. Calculation is based on the steady axisymmetric solution obtained with 30x30 basis functions.